

## Ⓞ Precipitation Sensitivity to Local Variations in Tropical Sea Surface Temperature

JIE HE,<sup>a,b,c</sup> NATHANIEL C. JOHNSON,<sup>a,b</sup> GABRIEL A. VECCHI,<sup>d,e</sup> BEN KIRTMAN,<sup>f</sup>  
ANDREW T. WITTENBERG,<sup>b</sup> AND STEPHAN STURM<sup>g</sup>

<sup>a</sup> Program in Atmospheric and Oceanic Sciences, Princeton University, Princeton, New Jersey

<sup>b</sup> Geophysical Fluid Dynamics Laboratory, Princeton, New Jersey

<sup>c</sup> School of Earth and Atmospheric Sciences, Georgia Institute of Technology, Atlanta, Georgia

<sup>d</sup> Geosciences Department, Princeton University, Princeton, New Jersey

<sup>e</sup> Princeton Environmental Institute, Princeton, New Jersey

<sup>f</sup> Rosenstiel School of Marine and Atmospheric Sciences, University of Miami, Miami, Florida

<sup>g</sup> Department of Mathematical Sciences, Worcester Polytechnic Institute, Worcester, Massachusetts

(Manuscript received 29 April 2018, in final form 4 September 2018)

### ABSTRACT

The driving of tropical precipitation by the variability of the underlying sea surface temperature (SST) plays a critical role in the atmospheric general circulation. To assess the precipitation sensitivity to SST variability, it is necessary to observe and understand the relationship between precipitation and SST. However, the precipitation–SST relationships from any coupled atmosphere–ocean system can be difficult to interpret given the challenge of disentangling the SST-forced atmospheric response and the atmospheric intrinsic variability. This study demonstrates that the two components can be isolated using uncoupled atmosphere-only simulations, which extract the former when driven by time-varying SSTs and the latter when driven by climatological SSTs. With a simple framework that linearly combines the two types of uncoupled simulations, the coupled precipitation–SST relationships are successfully reproduced. Such a framework can be a useful tool for quantitatively diagnosing tropical air–sea interactions. The precipitation sensitivity to SST variability is investigated with the use of uncoupled simulations with prescribed SST anomalies, where the influence of atmospheric intrinsic variability on SST is deactivated. Through a focus on local precipitation–SST relationships, the precipitation sensitivity to local SST variability is determined to be predominantly controlled by the local background SST. In addition, the strength of the precipitation response increases monotonically with the local background SST, with a very sharp growth at high SSTs. These findings are supported by basic principles of moist static stability, from which a simple formula for precipitation sensitivity to local SST variability is derived.


### 1. Introduction

Variations in tropical sea surface temperature (SST) play a crucial role in regulating global atmospheric variability (Trenberth et al. 1998). The impact of tropical SST is predominantly achieved through its local


influence on precipitation and convection (Barsugli and Sardeshmukh 2002), which affects not only nearby circulation through atmospheric latent heating (Gill 1980) but also remote climate through the propagation of planetary waves (Hoskins and Karoly 1981). With a strong response in local precipitation, certain tropical SST variations can exert worldwide climatic impacts, including droughts, floods, and intense hurricanes (Palmer 1986; Saji et al. 1999; McPhaden et al. 2006; Donnelly and Woodruff 2007).

From a thermodynamic perspective, we would expect greater precipitation sensitivity to SST variability at higher climatological SSTs, since SST anomalies over warmer regions should induce larger perturbations of boundary layer moist static energy, as low-level atmospheric moisture is

---

 Denotes content that is immediately available upon publication as open access.

---

 Supplemental information related to this paper is available at the Journals Online website: <https://doi.org/10.1175/JCLI-D-18-0262.s1>.

---

Corresponding author: Jie He, [jie.he@noaa.gov](mailto:jie.he@noaa.gov)

DOI: 10.1175/JCLI-D-18-0262.1

© 2018 American Meteorological Society. For information regarding reuse of this content and general copyright information, consult the [AMS Copyright Policy](#) ([www.ametsoc.org/PUBSReuseLicenses](http://www.ametsoc.org/PUBSReuseLicenses)).

expected to increase exponentially with SST. However, early observations of the SST–precipitation relationship showed a more complex picture. In scatterplots made from monthly mean data with SST on the  $x$  axis and convection on the  $y$  axis, a curve fit to the data steepens with a large positive slope as the SST reaches approximately 27.5°C but flattens and turns over with a negative slope at the highest SSTs (Gadgil et al. 1984; Graham and Barnett 1987; Bhat et al. 1996). Such an observation has engendered a number of studies, and it was later argued that the nonmonotonic SST–precipitation relationship is a result of the complex interplay between SST, circulation, and precipitation and should not be interpreted as a threshold of SST forcing at high SSTs (Waliser and Graham 1993; Zhang 1993; Lau et al. 1997).

We can think of tropical precipitation variability as partially driven by the variability of SST and partially by atmospheric (and land) internal dynamics, independent of the SST variability. Using atmosphere-only simulations with prescribed climatological SSTs, He et al. (2017) showed that a substantial amount of tropical precipitation variability can be generated without the influence of the temporal SST variations. Thus in a coupled atmosphere–ocean system, the intrinsic atmospheric forcing of the ocean is an important part of the interplay between SST and precipitation and must be accounted for when interpreting coupled SST–precipitation relationships (Trenberth and Shea 2005; Wu et al. 2006; He et al. 2017). As argued by Waliser and Graham (1993), the weak SST–precipitation relationship in the warm pool regions should reflect a strong influence of convective cloud on SST and not necessarily a weak SST forcing of precipitation. On the other hand, because the atmospheric intrinsic forcing of SST is inherently integrated into the coupled air–sea relationships, there remains a fundamental challenge in disentangling the SST-forced precipitation variability and the atmospheric intrinsic variability, and in quantitatively understanding the precipitation response to SST variability.

In this study, we show that atmosphere-only simulations forced with different boundary conditions (i.e., SSTs) can be used to disentangle the SST-forced response and the atmospheric intrinsic variability. Focusing on local SST–precipitation relationships, we aim to quantify precipitation sensitivity to local SST variability and to theoretically understand the relationship between this sensitivity and the background SST. Last, we construct a simple framework for the quantitative understanding of the coupled SST–precipitation relationships.

## 2. Data and simulations

We summarize the simulations here and will explain their purposes and briefly describe them again when

they are analyzed in the following sections. The results shown here include all seasons but the conclusions are consistent for individual seasons (not shown).

The main model used here is the Geophysical Fluid Dynamics Laboratory Forecast-Oriented Low Ocean Resolution model (GFDL-FLOR), which incorporates a 0.5° atmospheric (and land) model and a 1° ocean model (Vecchi et al. 2014). We perform three experiments with GFDL-FLOR: 1) a 200-yr fully coupled preindustrial control experiment, 2) a 200-yr atmosphere-only experiment with prescribed monthly mean SSTs and climatological mean sea ice concentrations taken from the coupled experiment, and 3) a 200-yr atmosphere-only experiment with prescribed climatological mean SSTs and sea ice concentrations from the coupled experiment.

We use two experiments from phase 5 of the Coupled Model Intercomparison Project (CMIP5; Taylor et al. 2012): 1) the coupled preindustrial control experiment (years 201–300) and 2) the 30-yr uncoupled atmosphere-only experiment driven by observed monthly mean SST and sea ice concentration from 1979–2008. Nine models that provide the necessary variables are used: BCC-CSM1.1, CanESM2, CNRM-CM5, HadGEM2-ES, IPSL-CM5B-LR, MIROC5, MPI-ESM-LR, MPI-ESM-MR, and MRI-CGCM3. All CMIP5 outputs are interpolated to a common 2° × 2° grid. All uncoupled experiments (including CMIP5 and GFDL-FLOR) that incorporate monthly varying SSTs are referred to as AMIP\_fullSST and those with climatological SSTs as AMIP\_climSST.

Two sets of observations are used, namely the Climate Prediction Center (CPC) Merged Analysis of Precipitation (CMAP; Xie and Arkin 1997) and the merged Hadley Centre–NOAA Optimal Interpolation SST (Hurrell et al. 2008) for the 1979–2008 period (to be consistent with the temporal range of the uncoupled CMIP5 simulations).

## 3. Coupled SST–precipitation relationships

Figure 1 shows the spatial distribution of the SST–precipitation local covariability diagnosed from observational estimates and CMIP5 coupled model simulations. In general, large SST–precipitation regression coefficients are located away from cold tongue regions, but the amplitude of the regression coefficients does not exactly follow the climatological SST. The largest regression coefficients appear near the west-central equatorial Pacific. This resembles the pattern of El Niño–Southern Oscillation (ENSO), which is known to induce large variations in precipitation. On the other hand, the regression coefficients are small in some of the warm pool regions (e.g., part of the off-equatorial Pacific convergence zones) and negative in some subtropical regions,

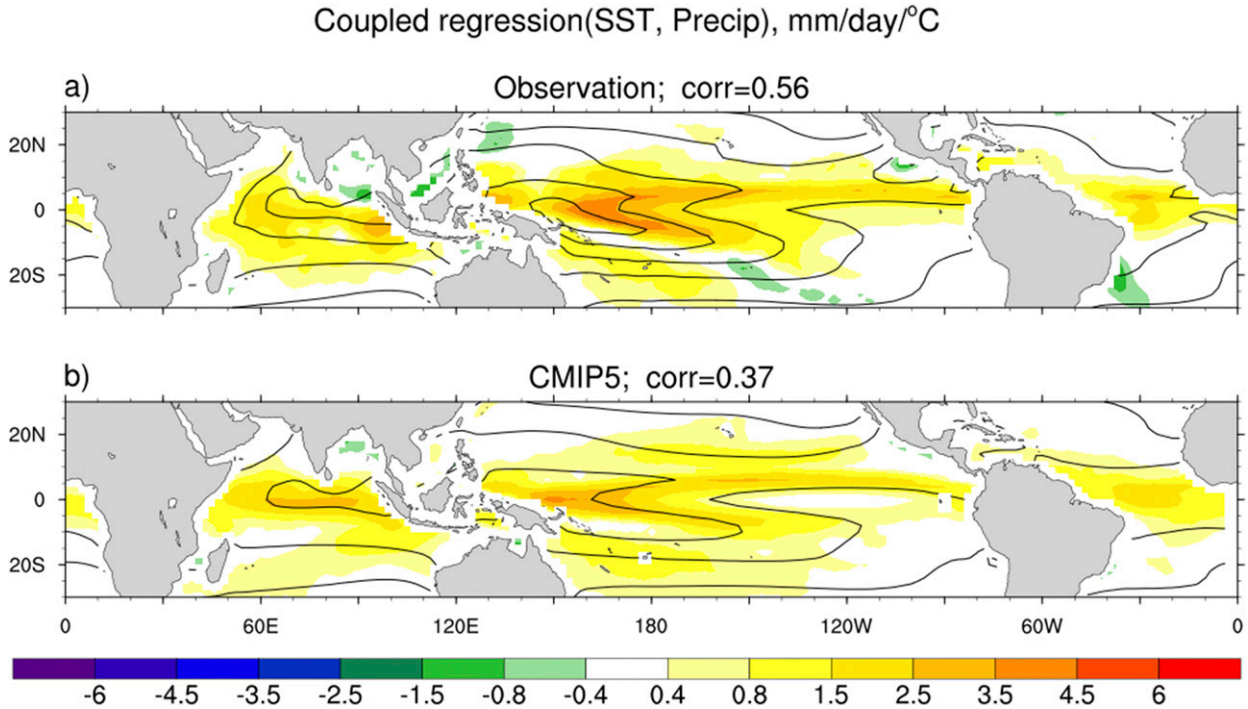


FIG. 1. Pointwise regression coefficients of anomalous monthly precipitation on SST from (a) observations and (b) the CMIP5 coupled multimodel mean. Contours show the climatological SST; contour levels are 22°, 26°, 28°, 29°, and 29.5°C. The (multimodel mean) spatial Spearman rank-order correlations between the SST–precipitation regression coefficients and the climatological SST are shown in the panel titles.

which can suggest a weak precipitation response to SST variability, a strong atmospheric intrinsic forcing of SST by convective clouds, or relatively strong remote forcing (Waliser and Graham 1993; Wu et al. 2006; He et al. 2017).

While we understand that the coupled SST–precipitation relationships result from a combination of SST forcing precipitation and precipitation forcing SST, it is difficult to directly observe and quantify either process as the two are inherently integrated in nature. This in turn creates a fundamental challenge in understanding and simulating the coupled climate. To expand on this issue, we first consider a heuristic one-dimensional linear model that couples local SST anomalies ( $SST'$ ) and precipitation anomalies  $P'$ :

$$P' = a \times SST' + F_p, \quad (1)$$

$$\frac{dSST'}{dt} = \frac{1}{c_w \rho_w H} (b \times P' + F_{SST}). \quad (2)$$

In this model, precipitation variability is partially driven by local SST anomalies with a positive forcing parameter  $a$  and partially by dynamics internal to the atmosphere or remote effects, as represented by  $F_p$ . As

shown by He et al. (2017), the atmospheric intrinsic precipitation variability resembles white noise at monthly and longer time scales. On the other hand, precipitation also influences SST, primarily through the cooling effect of cloud shading (Waliser and Graham 1993; Lau and Sui 1997), although downdrafts of cold, dry air also play a role (Sud et al. 1999). This precipitation forcing is captured with a negative value of  $b$  in Eq. (2). In this section, we set  $a$  equal to  $2 \text{ mm day}^{-1} \text{ °C}^{-1}$  and  $b$  equal to  $-3 \text{ W m}^{-2} (\text{mm day}^{-1})^{-1}$ , and for simplicity, we set both  $F_p$  and  $F_{SST}$  to Gaussian white noise. The values of these parameters are based on our climate model simulations as explained in section 7, where we apply a more realistic set of parameters to the linear model and will also consider the spatial characteristics of these parameters. The parameters  $c_w$ ,  $\rho_w$ , and  $H$  denote the specific heat capacity of water, seawater density, and mixed layer depth (set to 40 m), respectively.

We use the simple model to simulate the SST–precipitation relationship for a range of amplitudes of  $F_p$  and  $F_{SST}$ . As shown in Fig. 2, the regression coefficient is consistently smaller than the SST forcing  $a$  (except for  $F_p = 0$ ). In addition, the degree to which the regression coefficient deviates from  $a$  depends on the relative amplitude of  $F_p$  and  $F_{SST}$ . For the same SST

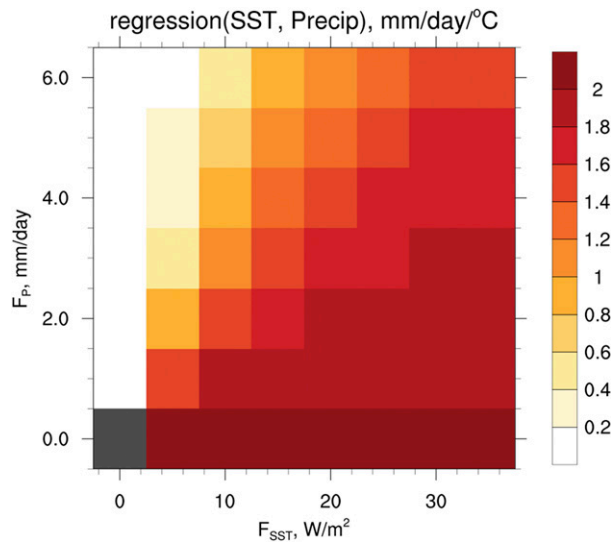


FIG. 2. Regression coefficients of monthly precipitation anomalies onto monthly SST anomalies from the simplified linear stochastic model for different amplitudes of stochastic precipitation variability  $F_P$  and dynamical SST variability  $F_{SST}$ . Note that the SST forcing of precipitation is set to  $2 \text{ mm day}^{-1} \text{ } ^\circ\text{C}^{-1}$ .

forcing parameter  $a$  and precipitation forcing parameter  $b$ , a large  $F_P$  leads to a small regression coefficient, whereas the opposite is true for  $F_{SST}$ . The various factors that are inherently integrated into the SST–precipitation relationship thus hinder the direct assessment of precipitation sensitivity to SST forcing from coupled SST–precipitation relationships. Moreover, the inability to quantify SST forcing and the other parameters in Eqs. (1) and (2) in turn creates a challenge for understanding and simulating the coupled SST–precipitation relationships.

#### 4. Simulated precipitation sensitivity to SST variability

How should we then quantify the precipitation sensitivity to SST forcing? Consider Eqs. (1) and (2) from a mathematical perspective. According to Eq. (1), the SST–precipitation regression would yield the correct forcing amplitude  $a$  if  $F_P$  were uncorrelated with SST'. However, this is not the case in a coupled system, as  $F_P$  impacts SST' via  $b \times P'$  in Eq. (2), which would result in a discrepancy between the regression coefficient and  $a$ . A straightforward solution is to use atmosphere-only models with prescribed SST evolution. In these simulations, the impact of atmospheric intrinsic variability on SST is disabled (Barsugli and Battisti 1998), so the SST–precipitation relationship only reflects the precipitation response to SST forcing.

Here, we analyze an ensemble of CMIP5 atmosphere-only simulations with prescribed monthly SSTs from

1979–2008 observations. To ensure the robustness of the results, these 30-yr simulations are discussed in conjunction with a 200-yr simulation from the uncoupled GFDL-FLOR model. The uncoupled GFDL-FLOR simulation is forced with the model's own monthly SSTs from the coupled preindustrial control run. We show in section 7 that such an experimental setup (AMIP\_fullSST) is able to accurately quantify the precipitation sensitivity in coupled climate models.

Consistent with the linear model, the SST–precipitation regression from the AMIP\_fullSST simulations (Fig. 3) is systematically larger than that in the coupled simulations (cf. Figs. 3 and 1). In contrast with the observations and CMIP5 coupled simulations, the uncoupled regression coefficients exhibit very similar patterns to the climatological SST, with spatial correlations exceeding 0.8. The largest regression coefficients generally are found over the warm pools, with only exceptions in the equatorial Atlantic. As discussed in section 5, these pointwise regression values primarily reflect the precipitation response to local SST variability.

The close pattern similarity between the precipitation sensitivity to SST forcing and the climatological SST indicates that the strength of SST forcing is largely determined by the climatological SST. The solid lines in Fig. 4a show the average SST forcing sorted by climatological SSTs. In both CMIP5 and GFDL-FLOR simulations, the SST forcing increases monotonically with the climatological SST (with the exception of CNRM-CM5 at SST = 29°C, possibly due to the shortness of the simulation). At high climatological SSTs, SST forcing grows drastically to high levels, but the point at which SST forcing starts to grow rapidly appears to vary among individual models (Fig. 5).

#### 5. Local versus nonlocal SST forcing

Precipitation responds to both local and remote SST anomalies. This section aims to clarify the physical meaning of the precipitation sensitivity diagnosed from pointwise SST–precipitation regression coefficients. Because the atmospheric intrinsic precipitation variability is uncorrelated with SST anomalies in the AMIP\_fullSST simulation, regressing precipitation onto SST effectively filters out the atmospheric intrinsic variability (which is not the case in the coupled simulation). Likewise, if the SST anomalies were random in space and time, the pointwise regression would average out the nonlocal SST forcing with only locally forced responses remaining. Nonlocality could arise, however, when the SST anomalies are temporally and spatially coherent.

In a separate uncoupled simulation in which SST anomalies are prescribed randomly, we found that its

## Uncoupled regression(SST, Precip), mm/day/°C

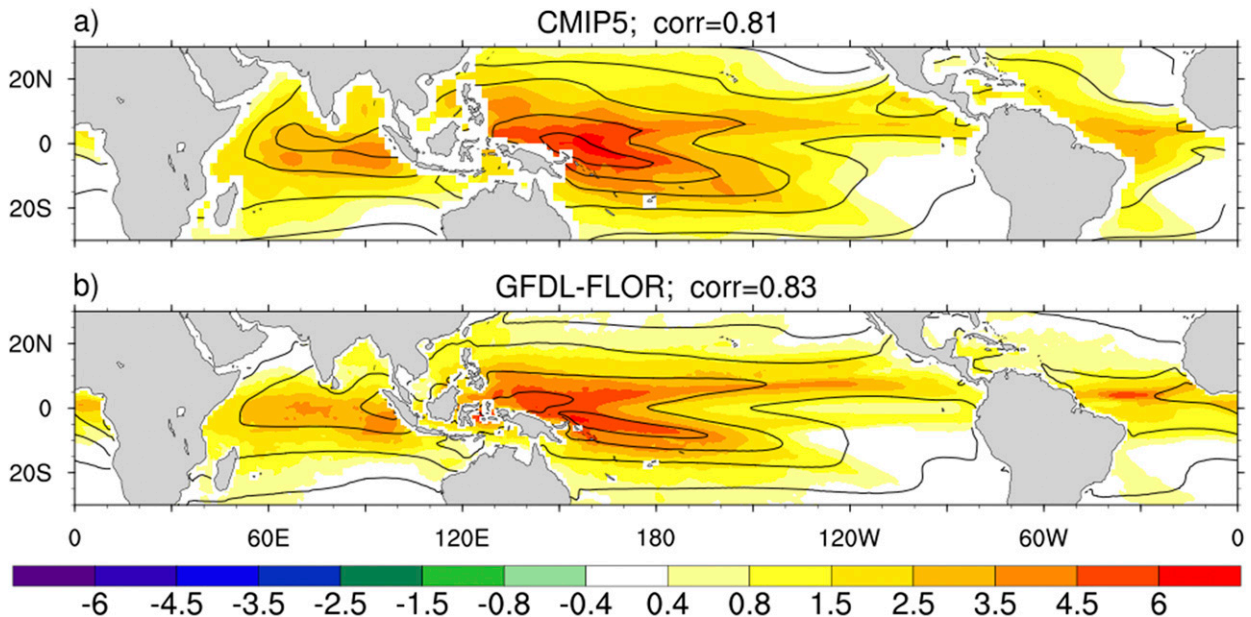


FIG. 3. Regression coefficients of anomalous monthly precipitation onto SST in the AMIP\_fullSST simulations from (a) the CMIP5 multimodel mean and (b) GFDL-FLOR. Contours are as in Fig. 1. The (multimodel mean) spatial Spearman rank-order correlations between the SST–precipitation regression and the climatological SST are shown in the panel titles.

SST–precipitation regression coefficients have similar structure and amplitude to those in a realistic SST setting (see Fig. S1 in the online supplemental material). This may not be intuitively predicted, since the realistic SST anomalies often occur with a repeating spatial structure, with ENSO being the most dominant case. In Fig. 6, we compare the SST–precipitation regression during the ENSO months and non-ENSO months. Discrepancies can be found on regional scales between the two cases, with ENSO acting to amplify the regression in the central western Pacific at the expense of the other ocean basins. This indicates that the remote SST forcing that is associated with the large-scale SST structure of ENSO can affect the local SST–precipitation relationship. However, the general features of the SST–precipitation regression are consistent during ENSO and non-ENSO months (Fig. 6d), both with the largest regression coefficients over warm pool regions. Therefore, the pointwise SST–precipitation regression coefficients to first order reflect precipitation sensitivity to local SST variability.

It should be noted, however, that the precipitation response to local SST variability at any given time should be considered in conjunction with the spatial structure of the SST anomaly, as the gradient of the SST anomalies can have great influence on surface wind,

particularly in the convective zone in the eastern Pacific (Lindzen and Nigam 1987; Back and Bretherton 2009). The local regression allows us to generalize the SST forcing as a time-averaged product, while neglecting the structure of such forcing that varies with time. Although we do not discuss the nonlocal SST forcing in this paper, it can be studied as well with atmosphere-only simulations.

## 6. A simple moist static energy model

Although the monotonic increase in precipitation sensitivity to climatological SST conforms with intuition, we still seek theoretical arguments for the rate at which the precipitation sensitivity increases. By neglecting horizontal advection and making a two-layer approximation that neglects vertical structure of convection, Neelin and Held (1987, hereafter NH87) derived a simple formula for tropical precipitation, in which precipitation is inversely proportional to the gross moist stability:

$$P \propto -q_s \nabla \cdot \mathbf{V}_s \approx \frac{F}{\Delta m}, \quad (3)$$

where  $q_s$  is the surface specific humidity,  $\mathbf{V}_s$  is the horizontal wind, and  $m$  is the moist static energy;  $F$  is

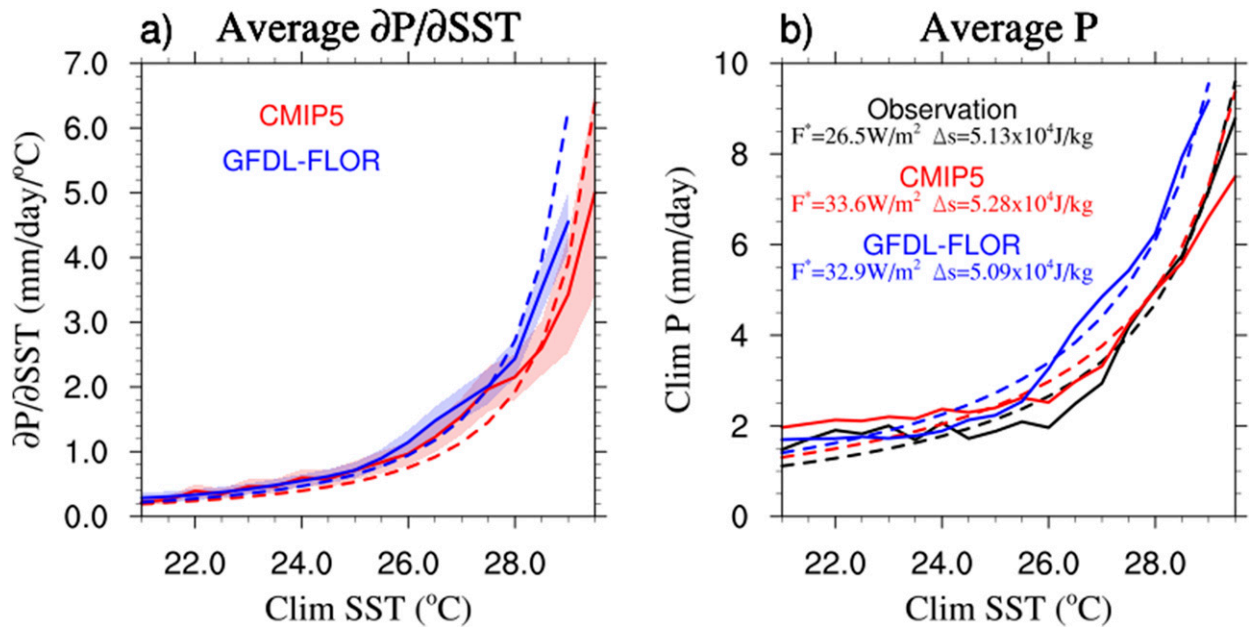


FIG. 4. (a) Average SST–precipitation regression coefficients from the CMIP5 (red) and GFDL-FLOR (blue) AMIP\_fullSST simulations sorted by climatological SST in  $0.5^{\circ}\text{C}$  bins (solid lines). Shading shows the uncertainty based on the CMIP5 intermodel standard deviation of the average SST–precipitation regression (red) and the 95% regression coefficient confidence interval for the GFDL-FLOR simulation (blue). Dashed lines show the corresponding values calculated from Eq. (5). (b) Average climatological precipitation sorted by climatological SST in  $0.5^{\circ}\text{C}$  bins (solid lines) and the corresponding values calculated from Eq. (4) (dashed lines) for observations (black), the CMIP5 multimodel mean (red), and the GFDL-FLOR simulation (blue). Note that GFDL-FLOR was run under preindustrial conditions and has a colder climatology than the uncoupled CMIP5 models that were run under present-day conditions.

constant and is derived from the energy flux difference between the tropopause and surface. The denominator on the right-hand side represents the gross moist stability (GMS; i.e.,  $\Delta m = m_t - m_s$ , where subscript  $t$  denotes the tropopause). Because moisture in the upper troposphere is negligible,  $\Delta m = \Delta s - L_v \times q_s$ , where  $L_v$  is the latent heat of condensation of water, and  $\Delta s$  is the dry static stability. Assuming constant tropopause temperature and that variations in surface moist static energy depend primarily on moisture rather than temperature (i.e., constant  $\Delta s$ ), the GMS is only determined by surface moisture, which depends essentially on SST. This way, SST becomes the sole ingredient of precipitation in Eq. (3).

Many subsequent studies have raised issues with NH87's theory, particularly regarding the parameterization of GMS as a function of SST. It was shown that the GMS actually does not correlate well with SST and involves intricate dynamical parameters that are not entirely driven by SST variability, such as convective depth and vertical velocity (Yu et al. 1998; Back and Bretherton 2006; Raymond et al. 2009). In addition, the assumption of constant tropopause temperature, which has been commonly used (e.g., Sobel and Bretherton 2000; Daleu et al. 2016), does not seem to hold, as

observations show that upper-tropospheric temperature variability far exceeds the SST variability (e.g., Fig. 3 of Stephens et al. 2004).

The mismatch between GMS and SST is expected, in part because GMS, just like precipitation, can be strongly influenced by atmospheric intrinsic dynamics. However, since our goal is to understand only the part of precipitation variability driven by SST variability, we can neglect all atmospheric intrinsic processes and only consider how variations in SST influence GMS (even though SST is not the only factor). Since the correlation between SST and tropospheric temperature quickly diminishes with height, we assume that SST only affects GMS through surface moist static stability. To calculate  $q_s$  from SST, we set surface relative humidity to 80% and surface air–sea temperature difference to  $1.5^{\circ}\text{C}$ . We define  $\Delta m = \Delta s - L_v \times q_s$  (where  $\Delta s$  is constant) as the SST-driven moist static stability (SMS) and rewrite Eq. (3) as

$$P(\text{SST}) \approx \frac{F^*}{\text{SMS}} = \frac{F^* \times q_s(\text{SST})}{\Delta s - L_v \times q_s(\text{SST})}, \quad (4)$$

where  $F^*$  is a constant. Equations (3) and (4) are the same except that Eq. (4) only applies to the SST-driven

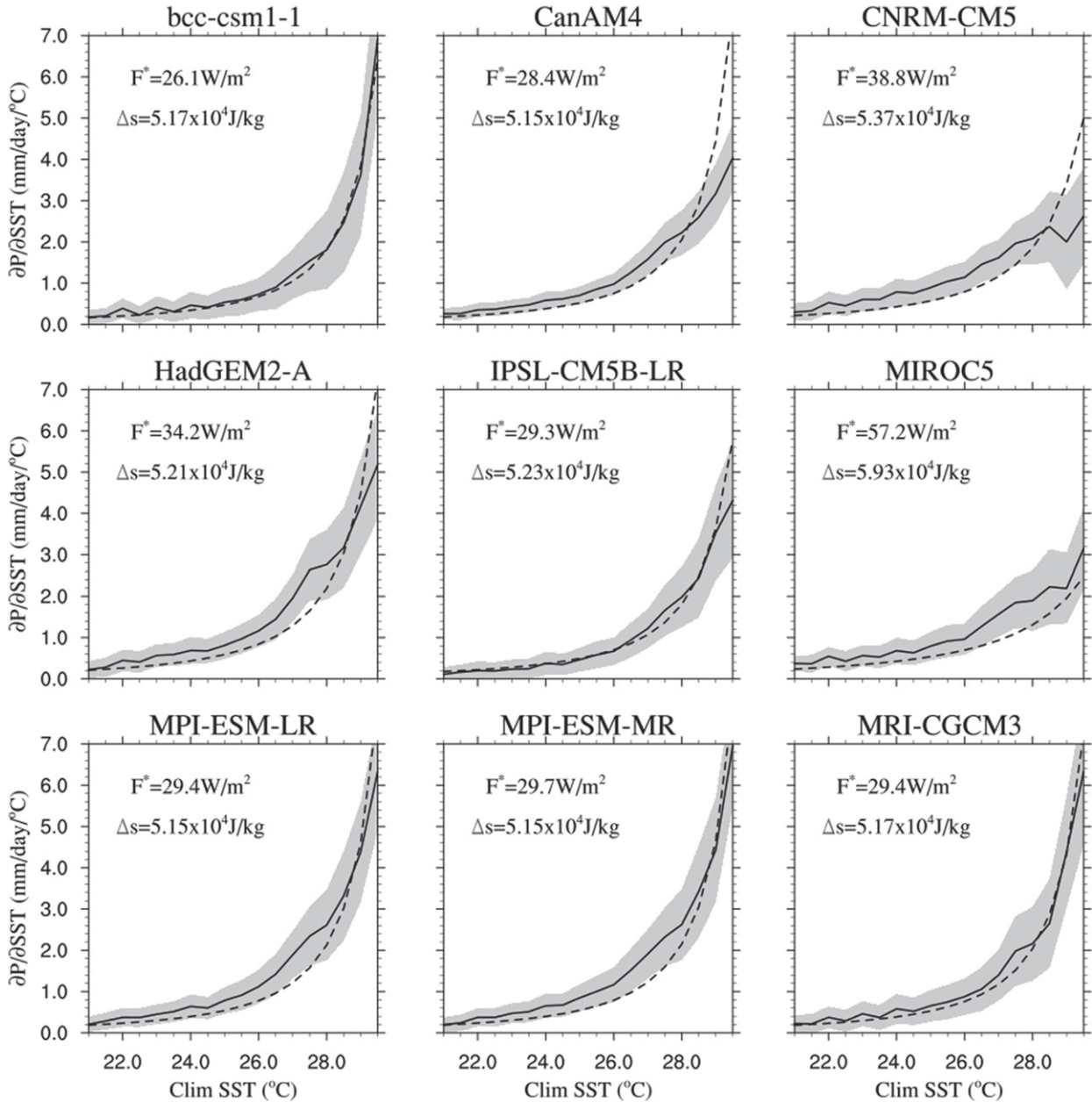


FIG. 5. Average SST–precipitation regression coefficients from individual uncoupled CMIP5 models sorted by climatological SST in 0.5°C bins. Shading shows the 95% regression coefficient confidence interval. Dashed lines show the corresponding values calculated from Eq. (7). See section 6 for definitions of  $F^*$  and  $\Delta s$ .

precipitation, which is related to SMS instead of GMS. This is a necessary conceptual adjustment for consolidating the mismatch between GMS and SST, and based on this adjustment we will test the utility of Eq. (4) for understanding precipitation sensitivity to SST variability.

It should be noted that there still remain two important caveats. First, the horizontal advection of moist static energy can be important for convection, particular on regional scales (Yu et al. 1998; Back and Bretherton

2006). Second, the SST-driven convections could have varying vertical structure and depth. Either process, if significant, would break the derivation of Eq. (4). It is possible that both processes can be important for individual SST-driven convective events but are arguably less so when it comes to the average sensitivity to SST anomalies, which is what we focus on here. Other simplifications associated with Eq. (4) include the lack of SST gradient forcing (Lindzen and Nigam 1987; Back and Bretherton

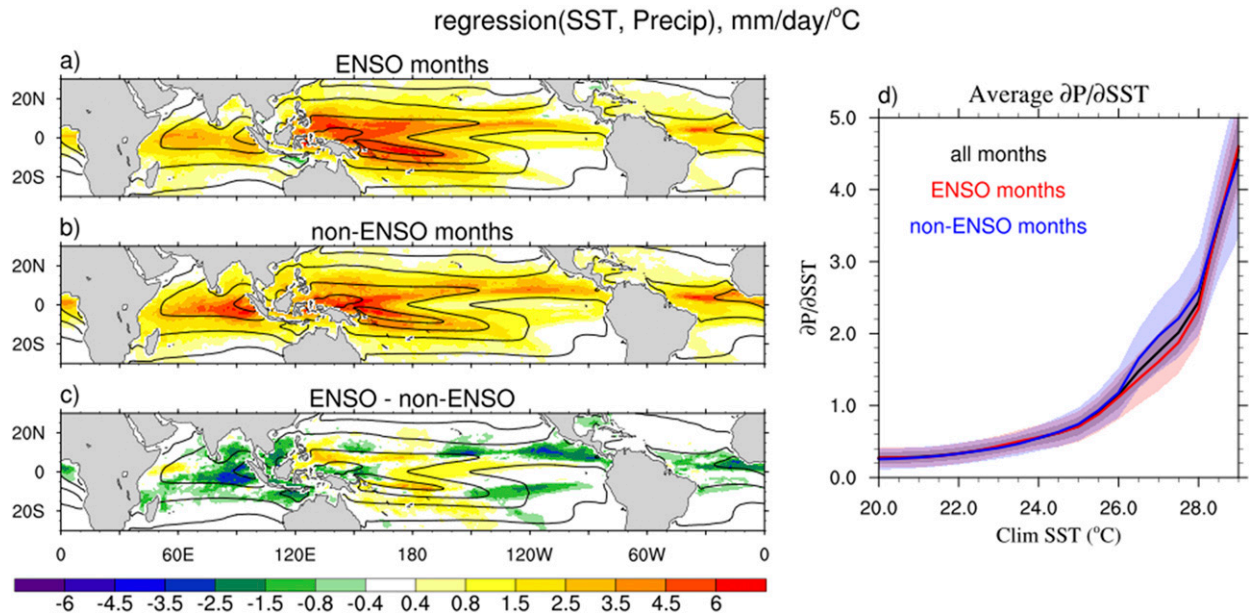


FIG. 6. SST–precipitation regression during (a) ENSO months and (b) non-ENSO months, and (c) the difference between the two from the GFDL-FLOR AMIP\_fullSST simulation. The ENSO (non-ENSO) months are defined as months when the amplitude of the Niño-3.4 SST anomaly is larger than 1 (smaller than 0.5) standard deviation. The standard deviation is calculated separately for each of the 12 months so the ENSO and non-ENSO months are not biased by season. There are approximately 800 ENSO and non-ENSO months in the 200-yr simulation. Contours show the climatological SST with the same contour style as Fig. 1. (d) The average precipitation sensitivity to SST sorted by 0.5°C climatological SST bins for ENSO months (red), non-ENSO months (blue), and all months (black). Shading shows the average 95% regression coefficient confidence interval for each climatological SST bin.

2009) and the lack of spatial variations in the tropospheric energy imbalance (i.e.,  $F$ ; Wang and Sobel 2011).

We use climatological data to estimate constants  $F^*$  and  $\Delta s$  in Eq. (4), based on a nonlinear least squares fit between the climatological  $q_s$  and precipitation. In the observations and models analyzed here,  $F^*$  varies around  $30 \text{ W m}^{-2}$  and  $\Delta s$  is approximately  $5 \times 10^4 \text{ J kg}^{-1}$  (Figs. 4b and 5), which is close to the tropical mean dry static energy difference between the tropopause and surface in the present climate (Fig. 7). The consistency between the estimated and the actual dry static stability offers some confidence in the physical basis of Eq. (4). As shown in Fig. 4b, Eq. (4) successfully captures the basic features of the time-mean precipitation that is binned onto the climatological SST, which was also shown in NH87. This suggests that Eq. (4) could be a reasonable starting point for studying the SST-forced precipitation response.

Using the Clausius–Clapeyron relationship between moisture and temperature, that is,  $\partial q_s/\partial SST \approx q_s \times 7\% \text{ } ^\circ\text{C}^{-1}$ , we obtain a simple formula for precipitation sensitivity to local SST variability:

$$\frac{\partial P}{\partial SST} \approx \frac{F^* \times \Delta s \times q_s(SST) \times 7\% \text{ } ^\circ\text{C}^{-1}}{[\Delta s - L_v \times q_s(SST)]^2}. \quad (5)$$

According to Eq. (5), the intensity of the SST forcing of precipitation increases monotonically with SST. The SMS, which appears in the denominator, is a crucial factor. At high SSTs (i.e., the warm pools), as  $L_v \times q_s$  approaches the critical limit set by the dry static stability  $\Delta s$ , the precipitation sensitivity becomes very large. (Note that the SMS is always positive at the monthly time scale.)

Next, we apply Eq. (5) to the climate model simulations. As shown by the dashed lines in Figs. 4a and 5, the simple formula reproduces the general structure of precipitation sensitivity to local SST variability from the climate models. Certain discrepancies are expected due to the simplicity of Eq. (5). In particular, Eq. (5) overestimates the SST forcing at very high climatological SSTs. As shown in Fig. 8, for those models for which SST forcing is overestimated by Eq. (5) at high SSTs (i.e., GFDL-FLOR, CanAM4, CNRM-CM5, and HadGEM2-A), their surface moisture clearly does not keep up with SST at high SSTs. Therefore, the overestimation is likely due to the assumption of constant relative humidity, which can be particularly problematic at high SSTs where the advection of dry air can be significant. In summary, the simple formula may serve as a starting point for understanding precipitation sensitivity and parameterizing



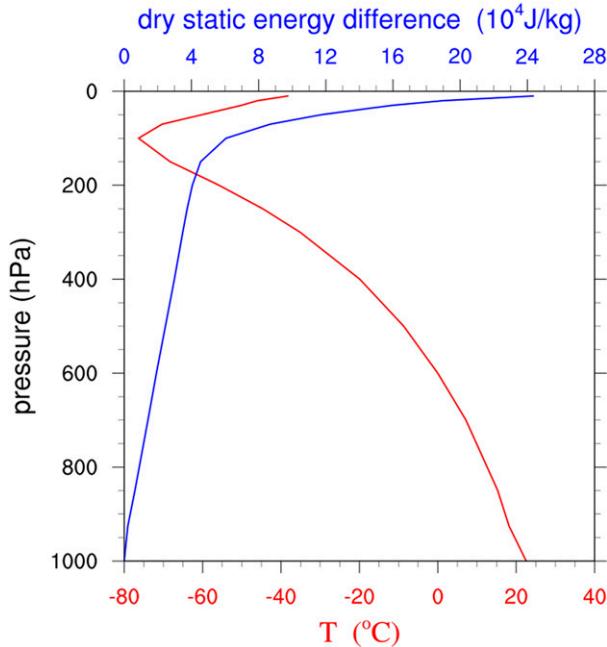


FIG. 7. Vertical profile of tropical mean temperature (red) and dry static energy deviation from the surface (blue) from the GFDL-FLOR AMIP\_fullSST simulation. Note the tropopause at 100 hPa, where the dry static energy deviation from the surface is approximately  $5 \times 10^4 \text{ J kg}^{-1}$ .

it as a function of the background SST. On the other hand, the simplifications used to derive Eq. (5), which we have described earlier, need to be investigated for more accurate applications.

## 7. A diagnostic framework for SST–precipitation interactions

To understand how SST–precipitation relationships emerge in a coupled system, we apply a more realistic version of the linear model [Eqs. (1) and (2)] by expanding it from one dimension ( $t$ ) to three dimensions ( $x, y, t$ ) and adjusting its parameters to match the GFDL-FLOR simulation. We set the SST forcing parameter  $a$  to the SST–precipitation regression from the GFDL-FLOR AMIP\_fullSST simulation (shown in Fig. 3b). We set the atmospheric intrinsic variability  $F_p$  to daily precipitation anomalies from an uncoupled GFDL-FLOR simulation forced with seasonally varying climatological SSTs from the coupled GFDL-FLOR control simulation (AMIP\_climSST). The use of a climatologically forced uncoupled simulation to estimate the atmospheric intrinsic variability was detailed and discussed in He et al. (2017).

We set the SST equation based on a linear quantification of the ocean mixed layer heat budget to take into

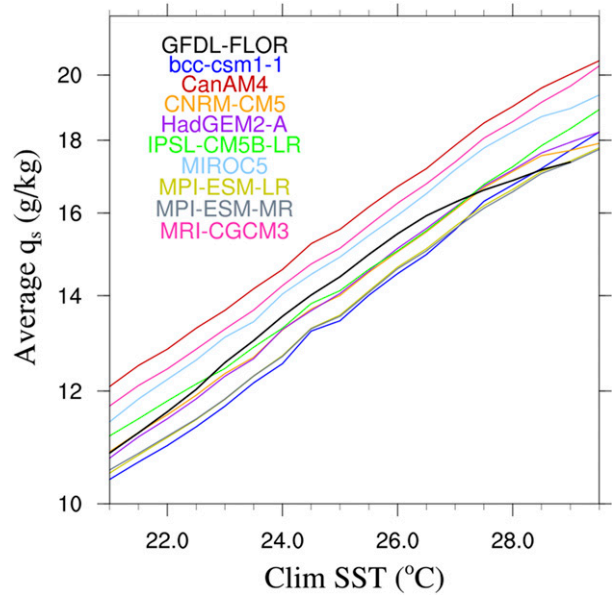


FIG. 8. Average surface specific humidity for  $0.5^\circ\text{C}$  climatological SST bins from each atmosphere-only simulation. The y axis is logarithmically spaced.

account SST variability that is driven by atmospheric energy fluxes and ocean dynamics. Specifically, the SST variability results from variations in surface shortwave radiation ( $\text{SW}'$ ), longwave radiation ( $\text{LW}'$ ), latent heat ( $\text{LH}'$ ), sensible heat ( $\text{SH}'$ ), and ocean dynamic forcing  $F_{\text{dyn}}$ . We assume that the surface shortwave radiation is primarily associated with precipitation variability (i.e.,  $\text{SW}' \approx b \times P'$ ). This is based on the fact that variations in surface shortwave radiation largely result from variations in cloud and (to a lesser degree) atmospheric moisture, which are closely related to precipitation (see Fig. S2 in the online supplemental material). We estimate parameter  $b$  using the regression coefficients of daily surface shortwave radiation anomalies onto daily precipitation anomalies from the GFDL-FLOR AMIP\_fullSST simulation. An alternative way to insert precipitation into the surface energy budget is to parameterize it into surface downwelling longwave radiation, since it has been shown from observations that the shortwave and longwave radiation associated with high cloud variability has similar amplitudes (e.g., Ramanathan et al. 1989). However in GFDL-FLOR, the shortwave forcing is much stronger (see Fig. S3 in the online supplemental material). Convection also cools SST through surface evaporation and sensible heat. Although these effects can be strong on certain occasions (Sud et al. 1999; Wu and Kirtman 2007), in general they are much weaker than the shortwave radiation effect (as shown by the evaporation–precipitation regression in Fig. S3c). We therefore decide to treat  $\text{LW}'$ ,  $\text{LH}'$ , and  $\text{SH}'$  separately from  $P'$ . In Eq. (2)  $F_{\text{SST}}$  then becomes

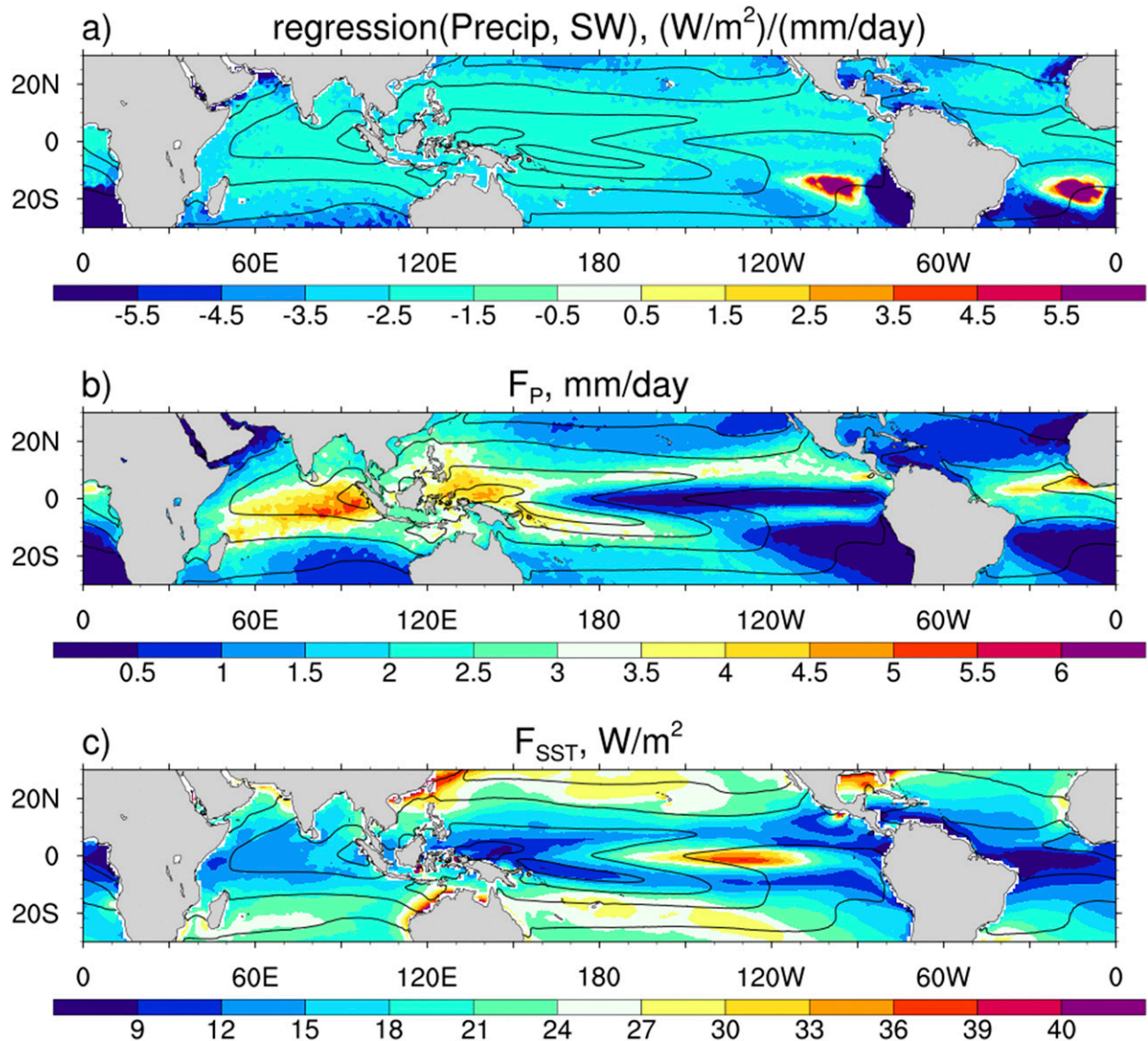


FIG. 9. (a) Precipitation forcing parameter  $b$  calculated as the regression coefficients of daily surface shortwave radiation anomalies onto daily precipitation anomalies from the GFDL-FLOR AMIP\_fullSST simulation. (b) Amplitude of  $F_P$  calculated as the standard deviation of monthly precipitation anomalies from the GFDL-FLOR AMIP\_climSST simulation. (c) Amplitude of  $F_{SST}$  based on a linear quantification of the ocean mixed layer heat budget (see section 7). Contours show the climatological SST from the coupled GFDL-FLOR simulation with the same contour style as Fig. 1.

$$F_{SST} = LW' + LH' + SH' + F_{dyn}.$$

We estimate  $LW'$ ,  $LH'$ , and  $SH'$  in the same way as  $P'$  by separating them into an SST-driven component and an intrinsic atmospheric component:

$$LW' = a_{LW} \times SST' + F_{LW},$$

$$LH' = a_{LH} \times SST' + F_{LH},$$

$$SH' = a_{SH} \times SST' + F_{SH},$$

where  $a_{LW}$ ,  $a_{LH}$ , and  $a_{SH}$  are specified as the regression of the respective monthly surface flux anomalies onto monthly SST anomalies from the GFDL-FLOR AMIP\_fullSST simulation forced with SST anomalies from the coupled GFDL-FLOR simulation;  $F_{LW}$ ,  $F_{LH}$  and  $F_{SH}$  are set to the respective daily surface flux anomalies from the GFDL-FLOR AMIP\_climSST simulation.

The parameter  $F_{dyn}$  represents the forcing by ocean dynamics, largely related to ENSO. Here, we estimate  $F_{dyn}$  using the part of heat flux at the bottom of the mixed layer ( $Q$  flux) that is linearly correlated with the

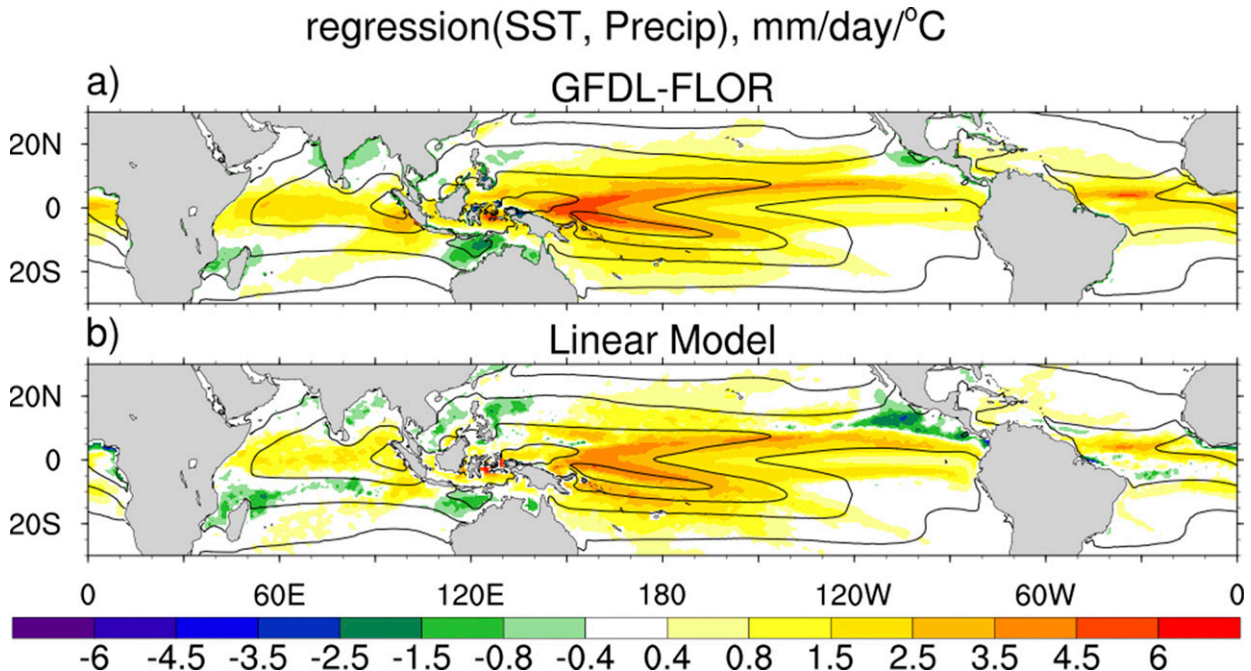


FIG. 10. Pointwise regression coefficients of anomalous monthly precipitation on SST from (a) the coupled GFDL-FLOR simulation and (b) the linear model simulation. Contours show the climatological SST from the coupled GFDL-FLOR simulation with the same contour style as Fig. 1.

$Q$  flux averaged over the Niño-3.4 region ( $5^{\circ}\text{S}$ – $5^{\circ}\text{N}$ ,  $120^{\circ}$ – $170^{\circ}\text{W}$ ) from the coupled GFDL-FLOR simulation. This is a modest estimation, since it does not account for the ocean dynamic forcing that is unrelated to ENSO.

Figure 9 illustrates the spatial distribution of the key parameters of the linear model. The precipitation forcing parameter  $b$  has a negative value and little spatial variation, except in part of the Southern Hemisphere subtropics where the strongest shortwave reflection is associated with nonprecipitating stratocumulus clouds resulting in a positive  $b$ . Because precipitation responds most strongly to SST variability in the warm pool regions, the amplitude of shortwave cooling  $b \times P'$  that is driven by SST anomalies is largest at high SSTs. This is consistent with the “cloud thermostat” hypothesis, which was proposed as the key mechanism for cooling SST hotspots (Ramanathan and Collins 1991; Wallace 1992; Hartmann and Michelsen 1993; Waliser 1996), although this mechanism likely applies only to local regions rather than the entire tropics as originally conceived (Pierrehumbert 1995). The atmospheric internal precipitation variability  $F_P$  has a very similar pattern as the climatological precipitation, with the largest amplitude in the warm pool regions (He et al. 2017). The value of  $F_{\text{SST}}$  is largest in the central equatorial Pacific due to active ocean circulation and in the subtropics due to

strong variability in wind-driven surface evaporation; it is generally small in the warm pool regions.

With the use of a realistic set of parameters, the linear model is able to reproduce the general features of the SST–precipitation relationship from the coupled GFDL-FLOR simulation (Fig. 10), including the large positive values at the central equatorial Pacific and the negative values in certain subtropical regions. In general, the regression coefficients are slightly lower in the linear model, which is likely due to its partial incorporation of ocean dynamics  $F_{\text{dyn}}$ . Combining the characteristics of the parameters illustrated in Figs. 3b and 9 and the idealized analysis in section 3, we can quantitatively understand the spatial features of the coupled SST–precipitation relationship. The strongest SST–precipitation relationship that is both observed (Graham and Barnett 1987; Lau et al. 1997) and simulated (Figs. 1 and 10a) in the western central equatorial Pacific results partially from a combination of relatively strong ocean dynamics and relatively weak atmospheric internal variability (compared to the Pacific warm pool), despite the fact that its SST forcing of precipitation is not the strongest. The Pacific warm pool has the strongest SST forcing, but the weak ocean dynamics and strong atmospheric internal variability lead to a relatively weak SST–precipitation relationship, particularly in the northern Pacific convergence

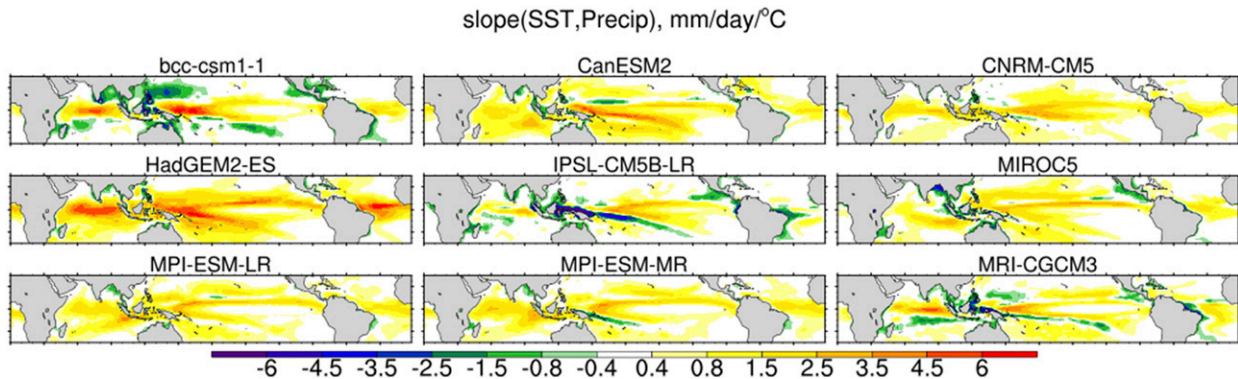


FIG. 11. Pointwise regression of monthly precipitation anomalies onto monthly SST anomalies from each coupled CMIP5 model. Notable differences can be found between these models and the observation (Fig. 1a).

zone and the poleward side of the southern Pacific convergence zone.

## 8. Implications and discussion

The climate is a fundamentally coupled system and requires coupled models to fully simulate its variability. On the other hand, the success of simulating a fully coupled system relies on understanding the oceanic forced climate response and the intrinsic atmospheric feedback, which are difficult to disentangle from coupled systems. Although the atmosphere-only simulations have been long criticized for their lack of two-way coupling, we have shown that their decoupled behavior can actually be used as a unique strength to study oceanic and atmospheric forcing in isolation. By incorporating the atmosphere-only simulations into a linear model, we have created a simple yet effective framework to dissect the complex nature of coupled air–sea relationships. The success of the linear framework demonstrates that the atmosphere-only simulations are useful tools for understanding precipitation sensitivity to SST variability.

State-of-the-art climate models are generally able to reproduce the basic structure of the observed air–sea relationship, but they exhibit substantial spread and biases on the spatial details (cf. Figs. 11 and 1a). These biases need to be understood not only to achieve better simulations of tropical climate variability, but also to improve short-term climate predictions (Wang et al. 2005). Highly simplified linear models have proven useful for understanding the basic nature of tropical air–sea interaction (Waliser and Graham 1993; Sobel and Gildor 2003; Wu et al. 2006), but the lack of realistic parameters makes them inadequate for quantitative analysis. By incorporating the linear model with atmosphere-only simulations, the simple framework

that is demonstrated here can potentially be an effective tool to diagnose the processes and sources of climate model biases relating to coupled air–sea relationships. In this regard, the framework adopted here may be a first step toward the development of process-oriented diagnostics that hone in on the mechanisms responsible for variations in the SST–precipitation relationships within climate models.

Such a framework may also help us to understand future changes in tropical air–sea relationships, which have already been detected in previous studies (Cai et al. 2014; Huang and Xie 2015). Future studies may benefit from the analysis of atmosphere-only simulations, which are able to quantify the changes in precipitation sensitivity to SST forcing. Based on the moist static stability theory, we showed that precipitation sensitivity is largely determined by the tropospheric dry static stability and SST patterns. Because both factors are projected to change in a warming climate (Johnson and Xie 2010; Xie et al. 2010), changes in precipitation sensitivity to SST variability are certainly expected (Huang et al. 2017) and will remain an important research subject.

*Acknowledgments.* We thank Clara Deser and Isaac Held for useful discussions. We also thank Adam Sobel and two anonymous reviewers for insightful reviews leading to improved presentation of the paper. We acknowledge the World Climate Research Programme’s Working Group on Coupled Modeling, which is responsible for CMIP5, and we thank the climate modeling groups for producing and making available their model output. This report was prepared by Jie He under award NA14OAR4320106 from the National Oceanic and Atmospheric Administration (NOAA), U.S. Department of Commerce. The statements, findings, conclusions, and recommendations are those of the author and do not necessarily reflect the views of the National

Oceanic and Atmospheric Administration, or the U.S. Department of Commerce. The GFDL simulations were conducted and archived on the NOAA's computer clusters that belong to the U.S. government. The outputs presented here are available from Jie He upon request.

## REFERENCES

- Back, L. E., and C. S. Bretherton, 2006: Geographic variability in the export of moist static energy and vertical motion profiles in the tropical Pacific. *Geophys. Res. Lett.*, **33**, L17810, <https://doi.org/10.1029/2006GL026672>.
- , and —, 2009: On the relationship between SST gradients, boundary layer winds, and convergence over the tropical oceans. *J. Climate*, **22**, 4182–4196, <https://doi.org/10.1175/2009JCLI2392.1>.
- Barsugli, J. J., and D. S. Battisti, 1998: The basic effects of atmosphere–ocean thermal coupling on midlatitude variability. *J. Atmos. Sci.*, **55**, 477–493, [https://doi.org/10.1175/1520-0469\(1998\)055<0477:TBEAO>2.0.CO;2](https://doi.org/10.1175/1520-0469(1998)055<0477:TBEAO>2.0.CO;2).
- , and P. D. Sardeshmukh, 2002: Global atmospheric sensitivity to tropical SST anomalies throughout the Indo-Pacific basin. *J. Climate*, **15**, 3427–3442, [https://doi.org/10.1175/1520-0442\(2002\)015<3427:GASTTS>2.0.CO;2](https://doi.org/10.1175/1520-0442(2002)015<3427:GASTTS>2.0.CO;2).
- Bhat, G. S., J. Srinivasan, and S. Gadgil, 1996: Tropical deep convection, convective available potential energy and sea surface temperature. *J. Meteor. Soc. Japan*, **74**, 155–166, [https://doi.org/10.2151/jmsj1965.74.2\\_155](https://doi.org/10.2151/jmsj1965.74.2_155).
- Cai, W., and Coauthors, 2014: Increasing frequency of extreme El Niño events due to greenhouse warming. *Nat. Climate Change*, **4**, 111–116, <https://doi.org/10.1038/nclimate2100>.
- Daleu, C. L., and Coauthors, 2016: Intercomparison of methods of coupling between convection and large-scale circulation: 2. Comparison over nonuniform surface conditions. *J. Adv. Model. Earth Syst.*, **8**, 387–405, <https://doi.org/10.1002/2015MS000570>.
- Donnelly, J. P., and J. D. Woodruff, 2007: Intense hurricane activity over the past 5,000 years controlled by El Niño and the West African monsoon. *Nature*, **447**, 465–468, <https://doi.org/10.1038/nature05834>.
- Gadgil, S., P. V. Joseph, and N. V. Joshi, 1984: Ocean–atmosphere coupling over monsoon regions. *Nature*, **312**, 141–143, <https://doi.org/10.1038/312141a0>.
- Gill, A. E., 1980: Some simple solutions for heat-induced tropical circulation. *Quart. J. Roy. Meteor. Soc.*, **106**, 447–462, <https://doi.org/10.1002/qj.49710644905>.
- Graham, N. E., and T. P. Barnett, 1987: Sea surface temperature, surface wind divergence, and convection over tropical oceans. *Science*, **238**, 657–659, <https://doi.org/10.1126/science.238.4827.657>.
- Hartmann, D. L., and M. L. Michelsen, 1993: Large-scale effects on the regulation of tropical sea surface temperature. *J. Climate*, **6**, 2049–2062, [https://doi.org/10.1175/1520-0442\(1993\)006<2049:LSEOTR>2.0.CO;2](https://doi.org/10.1175/1520-0442(1993)006<2049:LSEOTR>2.0.CO;2).
- He, J., C. Deser, and B. J. Soden, 2017: Atmospheric and oceanic origins of tropical precipitation variability. *J. Climate*, **30**, 3197–3217, <https://doi.org/10.1175/JCLI-D-16-0714.1>.
- Hoskins, B. J., and D. J. Karoly, 1981: The steady linear response of a spherical atmosphere to thermal and orographic forcing. *J. Atmos. Sci.*, **38**, 1179–1196, [https://doi.org/10.1175/1520-0469\(1981\)038<1179:TSLROA>2.0.CO;2](https://doi.org/10.1175/1520-0469(1981)038<1179:TSLROA>2.0.CO;2).
- Huang, P., and S.-P. Xie, 2015: Mechanisms of change in ENSO-induced tropical Pacific rainfall variability in a warming climate. *Nat. Geosci.*, **8**, 922–926, <https://doi.org/10.1038/ngeo2571>.
- , D. Chen, and J. Ying, 2017: Weakening of the tropical atmospheric circulation response to local sea surface temperature anomalies under global warming. *J. Climate*, **30**, 8149–8158, <https://doi.org/10.1175/JCLI-D-17-0171.1>.
- Hurrell, J. W., J. J. Hack, D. Shea, J. M. Caron, and J. Rosinski, 2008: A new sea surface temperature and sea ice boundary dataset for the Community Atmosphere Model. *J. Climate*, **21**, 5145–5153, <https://doi.org/10.1175/2008JCLI2292.1>.
- Johnson, N. C., and S.-P. Xie, 2010: Changes in the sea surface temperature threshold for tropical convection. *Nat. Geosci.*, **3**, 842–845, <https://doi.org/10.1038/ngeo1008>.
- Lau, K.-M., and C. H. Sui, 1997: Mechanisms of short-term sea surface temperature regulation: Observations during TOGA COARE. *J. Climate*, **10**, 465–472, [https://doi.org/10.1175/1520-0442\(1997\)010<0465:MOSTSS>2.0.CO;2](https://doi.org/10.1175/1520-0442(1997)010<0465:MOSTSS>2.0.CO;2).
- , H.-T. Wu, and S. Bony, 1997: The role of large-scale atmospheric circulation in the relationship between tropical convection and sea surface temperature. *J. Climate*, **10**, 381–392, [https://doi.org/10.1175/1520-0442\(1997\)010<0381:TROLSA>2.0.CO;2](https://doi.org/10.1175/1520-0442(1997)010<0381:TROLSA>2.0.CO;2).
- Lindzen, R. S., and S. Nigam, 1987: On the role of sea surface temperature gradients in forcing low-level winds and convergence in the tropics. *J. Atmos. Sci.*, **44**, 2418–2436, [https://doi.org/10.1175/1520-0469\(1987\)044<2418:OTROSS>2.0.CO;2](https://doi.org/10.1175/1520-0469(1987)044<2418:OTROSS>2.0.CO;2).
- McPhaden, M. J., S. E. Zebiak, and M. H. Glantz, 2006: ENSO as an integrating concept in Earth science. *Science*, **314**, 1740–1745, <https://doi.org/10.1126/science.1132588>.
- Neelin, J. D., and I. M. Held, 1987: Modeling tropical convergence based on the moist static energy budget. *Mon. Wea. Rev.*, **115**, 3–12, [https://doi.org/10.1175/1520-0493\(1987\)115<0003:MTCBOT>2.0.CO;2](https://doi.org/10.1175/1520-0493(1987)115<0003:MTCBOT>2.0.CO;2).
- Palmer, T. N., 1986: Influence of the Atlantic, Pacific and Indian Oceans on Sahel rainfall. *Nature*, **322**, 251–253, <https://doi.org/10.1038/322251a0>.
- Pierrehumbert, R. T., 1995: Thermostats, radiator fins, and the local runaway greenhouse. *J. Atmos. Sci.*, **52**, 1784–1806, [https://doi.org/10.1175/1520-0469\(1995\)052<1784:TRFATL>2.0.CO;2](https://doi.org/10.1175/1520-0469(1995)052<1784:TRFATL>2.0.CO;2).
- Ramanathan, V., and W. Collins, 1991: Thermodynamic regulation of ocean warming by cirrus clouds deduced from observations of the 1987 El Niño. *Nature*, **351**, 27–32, <https://doi.org/10.1038/351027a0>.
- , R. Cess, E. Harrison, P. Minnis, B. Barkstrom, E. Ahmad, and D. Hartmann, 1989: Cloud-radiative forcing and climate: Results from the Earth Radiation Budget Experiment. *Science*, **243**, 57–63, <https://doi.org/10.1126/science.243.4887.57>.
- Raymond, D. J., S. L. Sessions, A. H. Sobel, and Ž. Fuchs, 2009: The mechanics of gross moist stability. *J. Adv. Model. Earth Syst.*, **1**, 9, <https://doi.org/10.3894/JAMES.2009.1.9>.
- Saji, N. H., B. N. Goswami, P. N. Vinayachandran, and T. Yamagata, 1999: A dipole mode in the tropical Indian Ocean. *Nature*, **401**, 360–363, <https://doi.org/10.1038/43854>.
- Sobel, A. H., and C. S. Bretherton, 2000: Modeling tropical precipitation in a single column. *J. Climate*, **13**, 4378–4392, [https://doi.org/10.1175/1520-0442\(2000\)013<4378:MTPIAS>2.0.CO;2](https://doi.org/10.1175/1520-0442(2000)013<4378:MTPIAS>2.0.CO;2).
- , and H. Gildor, 2003: A simple time-dependent model of SST hot spots. *J. Climate*, **16**, 3978–3992, [https://doi.org/10.1175/1520-0442\(2003\)016<3978:ASTMOS>2.0.CO;2](https://doi.org/10.1175/1520-0442(2003)016<3978:ASTMOS>2.0.CO;2).
- Stephens, G. L., P. J. Webster, R. H. Johnson, R. Engelen, and T. L'Ecuyer, 2004: Observational evidence for the mutual

- regulation of the tropical hydrological cycle and tropical sea surface temperatures. *J. Climate*, **17**, 2213–2224, [https://doi.org/10.1175/1520-0442\(2004\)017<2213:OEFTMR>2.0.CO;2](https://doi.org/10.1175/1520-0442(2004)017<2213:OEFTMR>2.0.CO;2).
- Sud, Y. C., G. K. Walker, and K.-M. Lau, 1999: Mechanisms regulating sea-surface temperatures and deep convection in the tropics. *Geophys. Res. Lett.*, **26**, 1019–1022, <https://doi.org/10.1029/1999GL900197>.
- Taylor, K. E., R. J. Stouffer, and G. A. Meehl, 2012: An overview of CMIP5 and the experiment design. *Bull. Amer. Meteor. Soc.*, **93**, 485–498, <https://doi.org/10.1175/BAMS-D-11-00094.1>.
- Trenberth, K. E., and D. J. Shea, 2005: Relationships between precipitation and surface temperature. *Geophys. Res. Lett.*, **32**, L14703, <https://doi.org/10.1029/2005GL022760>.
- , G. W. Branstator, D. Karoly, A. Kumar, N.-C. Lau, and C. Ropelewski, 1998: Progress during TOGA in understanding and modeling global teleconnections associated with tropical sea surface temperatures. *J. Geophys. Res.*, **103**, 14 291–14 324, <https://doi.org/10.1029/97JC01444>.
- Vecchi, G. A., and Coauthors, 2014: On the seasonal forecasting of regional tropical cyclone activity. *J. Climate*, **27**, 7994–8016, <https://doi.org/10.1175/JCLI-D-14-00158.1>.
- Waliser, D. E., 1996: Formation and limiting mechanisms for very high sea surface temperature: Linking the dynamics and the thermodynamics. *J. Climate*, **9**, 161–188, [https://doi.org/10.1175/1520-0442\(1996\)009<0161:FALMFV>2.0.CO;2](https://doi.org/10.1175/1520-0442(1996)009<0161:FALMFV>2.0.CO;2).
- , and N. E. Graham, 1993: Convective cloud systems and warm-pool sea surface temperatures: Coupled interactions and self-regulation. *J. Geophys. Res.*, **98**, 12 881–12 893, <https://doi.org/10.1029/93JD00872>.
- Wallace, J. M., 1992: Effect of deep convection on the regulation of tropical sea surface temperature. *Nature*, **357**, 230–231, <https://doi.org/10.1038/357230a0>.
- Wang, B., Q. Ding, X. Fu, I.-S. Kang, K. Jin, J. Shukla, and F. Doblas-Reyes, 2005: Fundamental challenge in simulation and prediction of summer monsoon rainfall. *Geophys. Res. Lett.*, **32**, L15711, <https://doi.org/10.1029/2005GL022734>.
- Wang, S., and A. H. Sobel, 2011: Response of convection to relative sea surface temperature: Cloud-resolving simulations in two and three dimensions. *J. Geophys. Res.*, **116**, D11119, <https://doi.org/10.1029/2010JD015347>.
- Wu, R., and B. P. Kirtman, 2007: Regimes of seasonal air–sea interaction and implications for performance of forced simulations. *Climate Dyn.*, **29**, 393–410, <https://doi.org/10.1007/s00382-007-0246-9>.
- , —, and K. Pegion, 2006: Local air–sea relationship in observations and model simulations. *J. Climate*, **19**, 4914–4932, <https://doi.org/10.1175/JCLI3904.1>.
- Xie, P., and P. A. Arkin, 1997: Global precipitation: A 17-year monthly analysis based on gauge observations, satellite estimates, and numerical model outputs. *Bull. Amer. Meteor. Soc.*, **78**, 2539–2558, [https://doi.org/10.1175/1520-0477\(1997\)078<2539:GPAYMA>2.0.CO;2](https://doi.org/10.1175/1520-0477(1997)078<2539:GPAYMA>2.0.CO;2).
- Xie, S.-P., C. Deser, G. A. Vecchi, J. Ma, H. Teng, and A. T. Wittenberg, 2010: Global warming pattern formation: Sea surface temperature and rainfall. *J. Climate*, **23**, 966–986, <https://doi.org/10.1175/2009JCLI3329.1>.
- Yu, J.-Y., C. Chou, and J. D. Neelin, 1998: Estimating the gross moist stability of the tropical atmosphere. *J. Atmos. Sci.*, **55**, 1354–1372, [https://doi.org/10.1175/1520-0469\(1998\)055<1354:ETGMSSO>2.0.CO;2](https://doi.org/10.1175/1520-0469(1998)055<1354:ETGMSSO>2.0.CO;2).
- Zhang, C., 1993: Large-scale variability of atmospheric deep convection in relation to sea surface temperature in the tropics. *J. Climate*, **6**, 1898–1913, [https://doi.org/10.1175/1520-0442\(1993\)006<1898:LSVOAD>2.0.CO;2](https://doi.org/10.1175/1520-0442(1993)006<1898:LSVOAD>2.0.CO;2).